ELSEVIER

Journal of Power Sources 93 (2001) 32–40

JOURNAL OF POWER SOURCES

www.elsevier.com/locate/jpowsour

Design and material variation for an improved power output of AMTEC cells

M.A.K. Lodhi*, A. Daloglu

Department of Physics, Texas Technical University, Lubbock, TX 79409, USA

Received 12 May 2000; accepted 10 June 2000

Abstract

A number of design changes for improving the alkali metal thermo-electric converter (AMTEC) cell performance are investigated. In this study, both the material used in AMTEC cell and the dimensions of the cell are changed at the same time. Two different hot side temperatures, $T_{hot} = 1173$ K and $T_{hot} = 1023$ K, are tested. The condenser temperature, T_{cond}, is kept at 623 K. Results show that the maximum cell conversion efficiency and the maximum electrical power output take place for different cases. Comparing the PX-3A in operation at $T_{hot} = 1173$ K with the one proposed here, the maximum electrical power output and the maximum cell conversion efficiency increased by 43 and 44%, respectively. The corresponding values for $T_{hot} = 1023$ K are 46 and 48%.

Keywords: AMTEC; Heat losses; Power output; Efficiency; Design; Material; Power degradation

1. Introduction

The alkali metal thermo-electric converter (AMTEC) is receiving increasing attention as a direct energy conversion devise of high efficiency and high power density [1–28]. It has high conversion efficiency comparing the other thermo-electric energy conversion methods. It can provide efficiency close to the theoretical Carnot efficiency at relatively low temperatures. However, efficiencies for AMTEC currently achieved are limited to 15–20%. The high efficiency and high power density of AMTEC at relatively high heat-rejection temperature, around 600 K, and low heat source temperature, below 1200 K, make it an attractive option for space missions, air force applications and many terrestrial purposes. In the space exploration field, the planetary exploration missions have so far used thermo-electric energy conversion devices which have relatively low conversion efficiency (∼5–7%) compared to AMTEC. Accordingly those missions required larger and heavier general purpose heat source (GPHS). AMTEC being four to six times more efficient [5] would require less plutonium for GPHS, thus reducing the power system's mass by about 60%. It is expected that the continued interest in AMTEC cells will improve their efficiency, power density and reduce their time-dependent degradation.

The Air Force Research Laboratory (AFRL) has been operating AMTEC as test cells in a vacuum environment since 1997 summer. They are being manufactured by Advanced Modular Power Systems Inc. (AMPS) with design input from Orbital Sciences Corporation (OSC), Nichols Research Corporation (NRC) and AFRL. These tests are performed in a prototypical environment to evaluate design modifications, identify performance, and establish an endurance data-base.

2. AMTEC PX-3A apparatus

A brief design description of AMTEC cell and its working is given here. Fig. 1 shows a typical PX type AMTEC cell. Our investigations are directed to the PX-3A type cell which contains five Beta' Alumina Solid Electrolyte (BASE) tubes in series and operates in a vapor–vapor mode, which means that sodium is in the vapor state on the low and high pressure sides of the BASE. Liquid sodium is wicked from the condenser and evaporated to the vapor at the evaporator in the space also shared by the high pressure side (inside) of the BASE tubes. The BASE tubes have two thin, porous electrodes of TiN, anode and cathode, on the inner and outer surfaces, respectively. The inner and outer electrodes are

* Corresponding author. Tel.: +1-806-742-3778; fax: +1-806-742-1182.
E-mail address: b5mak@ttacs.ttu.edu (M.A.K. Lodhi).

0378-7753/01/$ – see front matter
PII: S0378-7753(00)00538-3

Nomenclature

B	temperature independent exchange current
P_{out}	electrical energy generated by the cell (W)
Q_{artery}	conducted heat to condenser through artery (W)
Q_{cond}	latent heat of condensation of sodium (W)
Q_{input}	amount of heat supplied to the cell (W)
Q_{insul}	heat losses to ambient through cell wall and insulation (W)
Q_{rcond}	net radiated energy to condenser (W)
Q_{wall}	conducted heat to condenser through cell wall (W)
R_{BASE}	BASE resistivity
T_{cold}	condenser temperature (K)
T_{hot}	hot plate temperature (K)
η	efficiency

each contacted by a current collector which collects electrons at the anode (high pressure side of the BASE), conducts them through an external load, and supplies them for recombination with the sodium ions at the cathode (low pressure side of the BASE). The heat is supplied through the hot plate and the cell is tested in vacuum. The material and geometrical dimensions of this cell are given in Table 1.

PX-3A type cell consists of different materials used for cell components. These components work at high temperature in sodium environment. Because of the large number of potential chemical interaction at high temperature, the degradation in cell performance is very likely. The experimental data for 18,000 h operation time of PX-3A AMTEC cell obtained from AFRL shows degradation of the cell by 48%, see Fig. 2 [29].

Table 1
Design parameters of PX-3A cell

Cell diameter (mm)	31.75
Cell height (mm)	101.6
Evaporator type	Deep cone
Evaporator elevation (mm)	5.18
Evaporator standoff thickness (mm)	0.71
Evaporator standoff material	SS
Standoff rings (mm)	1.1
Rings material	Ni
Stud area (mm^2)	38
Stud material	SS
Number of BASE tubes	5
Tube length	32
Electrode/tube (mm^2)	600
Tube braze material	TiNi
Current collector	60-mesh Mo
Feedthrough braze	TiCuNi
Radiation shield type	Circular
Shield material	SS
Condenser type	Creare
Hot side	SS
Cell wall	SS
Initial test date	7/9/97
Operation (h)	18,000

3. Improved cell strategy

The recent studies of material parameter and design configuration of AMTEC [30–33] indicate that the adequate amount of heat supply from the hot plate to the evaporator is important while allowing sodium vapor to pass. This supply of heat depends greatly on the material, dimensions of stud and braze, and the distance from the hot plate to the evaporator. The appropriate changes in the material and

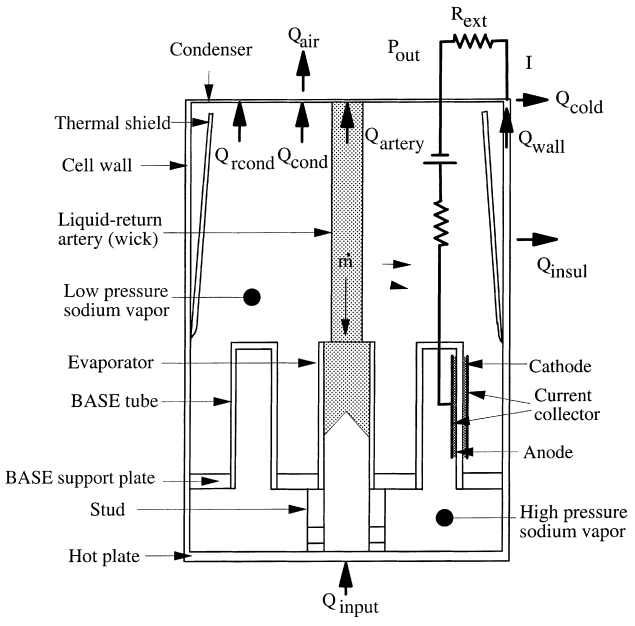

Fig. 1. A schematic diagram of vapor-anode AMTEC cell.

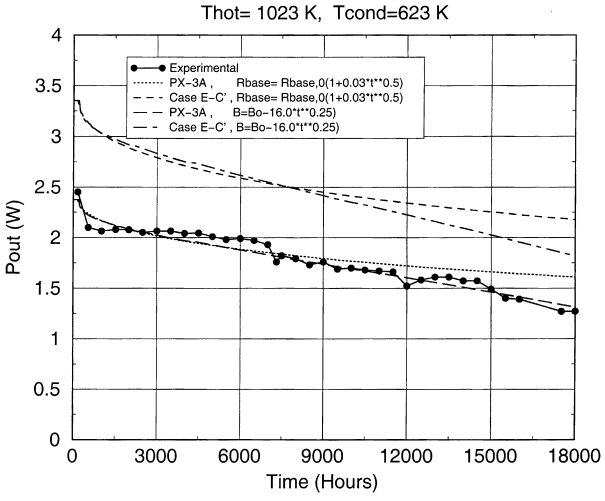

Fig. 2. PX-3A degradation over time.

cell configuration enhance the thermal conductance between the hot end of the cell and the evaporator, which in turn results in significant gain of thermal conversion efficiency. It is also noticed that the cell performance is vitally dependent on the ultimate temperature of the material in use particularly at or near the hot end of the cell, as the hot end temperature governs the cell performance primarily. The variation in the cell height, keeping cell diameter and the length of the BASE tubes, affects the radiation and conduction parasitic losses inversely and hence the cell power output directly. The effect of the variation in the length of the BASE tube on the heat losses from different components varies but over all the cell efficiency increases for increasing the length of the BASE tubes.

In summary for an over all improved performance of the AMTEC cell several issues have been identified by theoretical and experimental investigation on design strategies and material parameter variation. In this work we have addressed both effects, namely the geometrical configuration of the cell and material performance. For improved efficiency and more power output we primarily focus our attention on (i) supplying adequate heat for conversion, while maintaining appropriate temperature distribution, optimization of heat flow from the hot plate to the evaporator and BASE tubes, (ii) using those materials which allow higher hot side temperature, (iii) minimizing the parasitic heat losses all the way from hot side of the cell to the condenser, and (iv) minimizing the internal electrical losses.

4. Effect of individual parametric variation

The different design techniques can be applied to improve the cell performance. In this study, minimization of heat losses from the AMTEC cell and optimization of heat flow through the hot plate are mostly considered. High thermal conductivity and ultimate temperature materials are used for hot region components (hot plate, stud, braze, and evaporator) to increase the amount of the heat passing through the cell. Low thermal conductivity materials are used for the cooler region components (condenser, cell wall, artery, and shield) to decrease heat losses.

Materials for individual cell components are used the following way.

- Case A: material for hot plate, stud and evaporator is changed from SS to Ni.
- Case B: in addition to case A, the material for condenser, artery, shield and cell wall is changed from SS to Inconel.
- Case C: in addition to case B, the emissivity of sodium film is changed from 0.05 to 0.025; because the emissivity of liquid sodium is given as 0.02 in [34].
- Case D: in addition to case C, cell wall and artery coated with Rh ($\varepsilon = 0.06$).
- Case E: in addition to case D, material for cell wall above the BASE tube is changed from SS to ceramic, ZrO_2.
- Case F: in addition to case E, perfect insulator is assumed as a insulation material instead of Molded Mink-K.

Design configuration of individual cell components are changed in the following manner.

- Case A′: the length of the cell is increased from 101.6 to 127 mm (25%).
- Case B′: in addition to case A, the cell diameter is decreased from 31.75 to 26.99 mm (15%).
- Case C′: in addition to case A, the cell diameter is increased from 31.75 to 36.51 mm (15%).
- Case D′: in addition to case B, the cross-section area of the stud is increased from 37.7 to 120.0 mm^2 (218%).
- Case E′: in addition to case A, the cross-section area of the stud is increased from 37.7 to 120.0 mm^2 (218%).
- Case F′: in addition to case D, the length of the BASE tube decreased from 31.75 to 28.58 mm (10%).
- Case G′: in addition to case D, the length of the BASE tube increased from 31.75 to 36.51 mm (15%), and the length of the electrodes is increased from 25.40 to 33.02 mm (30%).

5. Results and discussion

These geometrical and material changes are tested in a code developed in Standard Fortran 77. This code mainly consists of three models: vapor pressure loss model, cell electrochemical and electrical model, and radiation/conduction heat transfer model [35]. The theoretical maximum electrical power output and maximum cell conversion efficiency for the PX-3A cell evaluated at $T_{hot} = 1173$ K are obtained as 4.99 W and 12.98%. The corresponding values for the same cell are 2.06 W and 9.30% when evaluated at $T_{hot} = 1023$ K.

The effects of the design changes on the maximum electrical power output and maximum cell conversion efficiency are given Tables 2–5 for two different hot side temperatures. The case F–case C′ gives the maximum electrical power although the case F–case G′ gives the maximum power for two different hot side temperatures. For $T_{hot} = 1023$ K, the maximum electrical power output and maximum cell conversion efficiency reach to 3.11 W and 18.83%, respectively; whereas for $T_{hot} = 1173$ K they give higher values as 6.59 W and 24.24%. Case B′ gives the minimum electrical power output because of the smaller cell diameter although case C′ gives the minimum cell conversion efficiency because of the larger cell diameter. The cell with larger diameter allows more heat to pass through the cell but heat losses increase with increasing wall area, which cause the cell conversion efficiency to decrease.

Radial heat loss to the environment through the cell wall and insulation, Q_{insul}, axial heat losses to the condenser through the artery, Q_{artery}, the same through the cell wall, Q_{wall}, and the net heat radiation to condenser, Q_{rcond}, as indicated in Fig. 1, are given as a function of current at

Table 2
The maximum cell power output[a]

Changes in geometry	Changes in material						
	PX-3A	Case A	Case B	Case C	Case D	Case E	Case F
PX-3A	4.490	5.971	5.995	6.012	6.109	6.135	6.253
Case A′	4.528	5.994	6.011	6.023	6.104	6.114	6.268
Case B′	3.996	5.333	5.341	5.345	5.381	5.384	5.508
Case C′	4.733	6.228	6.256	6.277	6.401	6.419	6.589
Case D′	4.197	5.467	5.475	5.479	5.515	5.518	5.636
Case E′	4.759	6.148	6.148	6.165	6.258	6.267	6.415
Case F′	4.363	5.590	5.596	5.600	5.631	5.629	5.731
Case G′	4.457	6.058	6.067	6.071	6.112	6.122	6.252

[a] $T_{hot} = 1173$ K, $T_{cond} = 623$ K.

Table 3
The maximum cell efficiency[a]

Changes in geometry	Changes in material						
	PX-3A	Case A	Case B	Case C	Case D	Case E	Case F
PX-3A	12.980	14.380	14.790	15.020	16.640	18.090	22.990
Case A′	13.394	14.819	15.161	15.330	16.857	18.003	23.825
Case B′	13.873	15.290	15.547	15.636	16.739	17.719	23.405
Case C′	12.363	13.771	14.180	14.431	16.319	17.586	23.432
Case D′	14.178	15.456	15.713	15.803	16.906	17.871	23.543
Case E′	13.698	14.990	15.329	15.499	17.031	18.176	23.967
Case F′	14.436	15.654	15.912	16.002	17.130	18.119	23.687
Case G′	14.836	16.394	16.650	16.733	17.789	18.654	24.243

[a] $T_{hot} = 1173$ K, $T_{cond} = 623$ K.

Table 4
The maximum cell power output[a]

Changes in geometry	Changes in material						
	PX-3A	Case A	Case B	Case C	Case D	Case E	Case F
PX-3A	2.060	2.824	2.836	2.844	2.893	2.898	2.965
Case A′	2.080	2.832	2.839	2.845	2.888	2.884	2.973
Case B′	1.840	2.533	2.536	2.538	2.556	2.552	2.619
Case C′	2.160	2.920	2.934	2.943	3.009	3.007	3.106
Case D′	1.950	2.606	2.609	2.611	2.629	2.625	2.689
Case E′	2.200	2.916	2.924	2.929	2.971	2.968	3.053
Case F′	2.020	2.669	2.671	2.673	2.688	2.683	2.739
Case G′	2.070	2.894	2.898	2.900	2.920	2.920	2.992

[a] $T_{hot} = 1023$ K, $T_{cond} = 623$ K.

Table 5
The maximum cell efficiency[a]

Changes in geometry	Changes in material						
	PX-3A	Case A	Case B	Case C	Case D	Case E	Case F
PX-3A	9.303	10.602	10.914	11.066	12.183	13.246	17.766
Case A′	9.600	10.917	11.177	11.283	12.382	13.233	18.571
Case B′	9.860	11.178	11.378	11.431	12.217	12.982	18.118
Case C′	8.860	10.147	10.458	10.621	11.977	12.885	18.272
Case D′	10.120	11.328	11.529	11.582	12.370	13.132	18.245
Case E′	9.870	11.072	11.333	11.440	12.542	13.391	18.706
Case F′	10.360	11.516	11.718	11.771	12.580	13.356	18.386
Case G′	10.610	12.068	12.269	12.319	13.075	13.763	18.827

[a] $T_{hot} = 1023$ K, $T_{cond} = 623$ K.

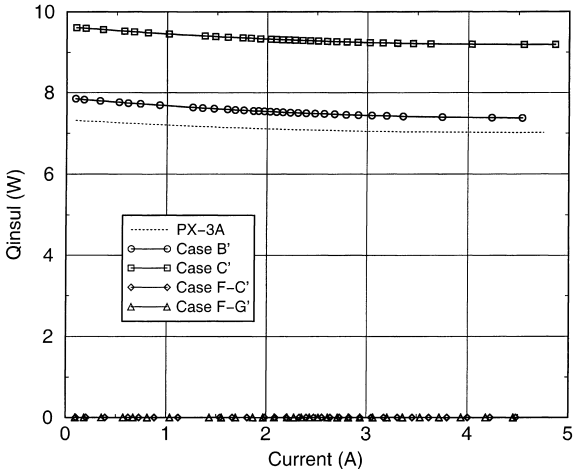

Fig. 3. Heat losses to ambient through cell wall and insulation ($T_{hot} = 1173$ K).

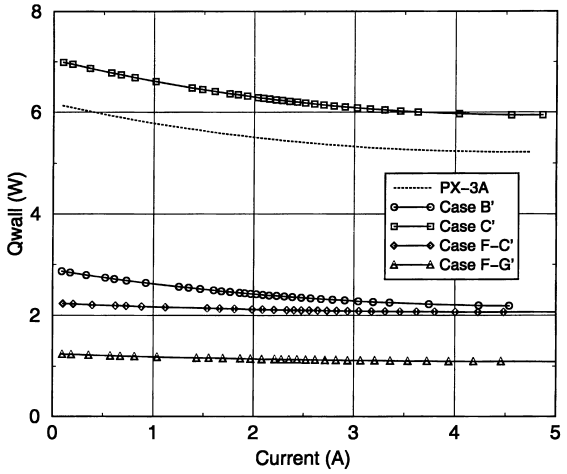

Fig. 5. Conducted heat to condenser through cell wall ($T_{hot} = 1173$ K).

$T_{hot} = 1173$ K in Figs. 3–6. In these figures the dotted line shows the values for PX-3A in operation. As it is expected we notice in Fig. 3 that Q_{insul} becomes zero in case F–C′ and case F–G′ where the insulator for cell wall is assumed the perfect (adiabatic). In case C′, Q_{insul} is high because of larger values of cell diameter and length. For all the investigated cases, heat losses through the artery, Q_{artery} in Fig. 4, show lower values than that of PX-3A cell in operation. This is expected; for the thermal resistance varies directly as the length. In Fig. 5, heat loss through cell wall, Q_{wall}, gives similar results as Q_{artery}, but it takes higher value for case C′ because of larger cell diameter (larger cross-sectional area). In Fig. 6 for case C′ and case F–C′, the net heat radiation to condenser, Q_{rcond}, increases as it depends directly on the cell diameter and the surface area.

The amount of heat supplied to the cell, Q_{input}, the electrical power generated by the cell, P_{out}, and the cell conversion efficiency, η, are shown in Figs. 7–9. The behavior of heat input to the cell versus current is given in Fig. 7.

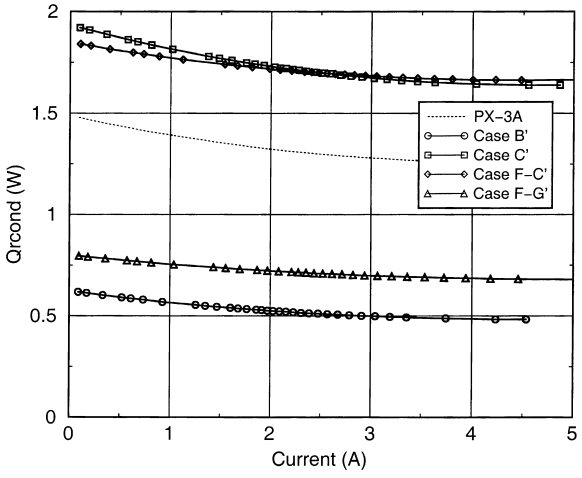

Fig. 6. Net heat radiation to condenser ($T_{hot} = 1173$ K).

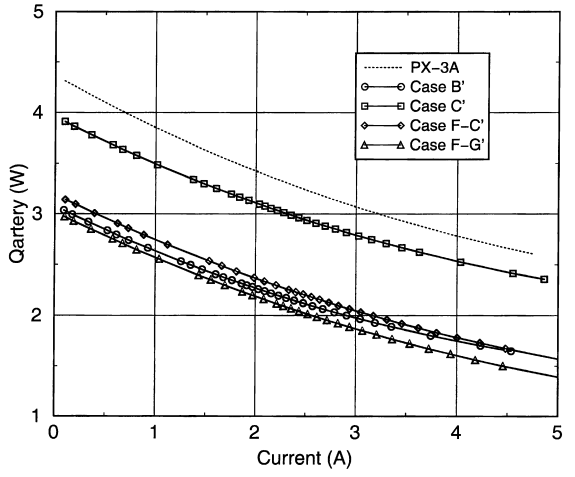

Fig. 4. Conducted heat to condenser through artery ($T_{hot} = 1173$ K).

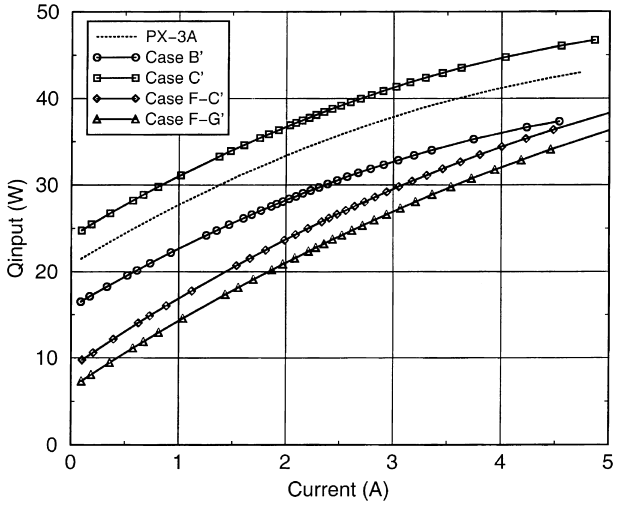

Fig. 7. The heat supplied to the AMTEC cell ($T_{hot} = 1173$ K).

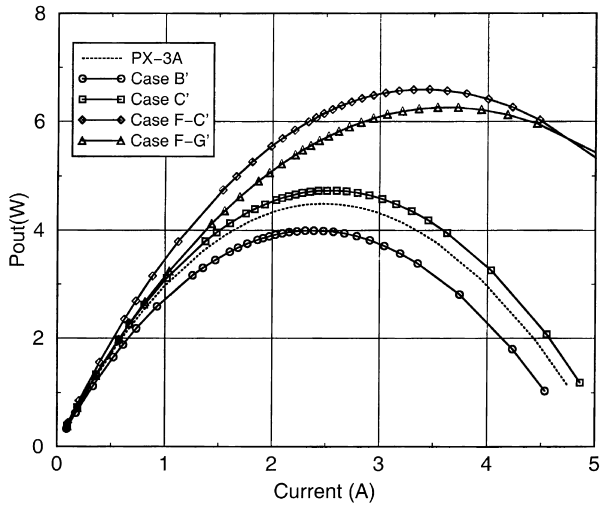

Fig. 8. The electrical power generated by the cell ($T_{hot} = 1173$ K).

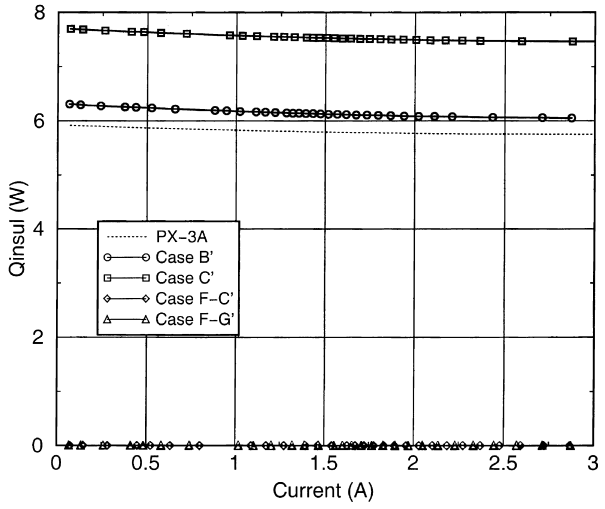

Fig. 10. Heat losses to ambient through cell wall and insulation($T_{hot} = 1023$ K).

The maximum heat transmits into the cell in case C′, because of larger cell diameter (larger hot plate surface area). Although the cell diameter is the same for case F–C′ as for case C′, the amount of heat supplied to the cell, Q_{input}, in this case, decreases because the heat losses from the cell are less as seen in Figs. 3–6. In Figs. 8 and 9, the electrical power generated by the cell, and the cell conversion efficiency are both given as functions of current. We note that the minimum electrical power in case B′, but the minimum conversion efficiency in case C′. This is because of the smaller diameter in case B′ and larger diameter in case C′. Although the maximum electrical power output is in case E–C′ (6.42 W), the case E–G′ gives maximum conversion efficiency (18.65%). The maximum electrical power and the maximum cell conversion efficiency increase by 43 and 44%, respectively. For $T_{hot} = 1023$ K, similar results are obtained and are given in Figs. 10–16. The maximum electrical power reached to 3.01 W, and the maximum cell

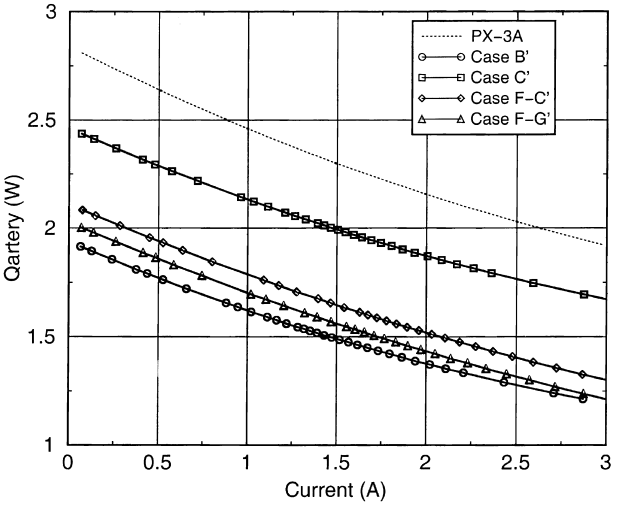

Fig. 11. Conducted heat to condenser through artery ($T_{hot} = 1023$ K).

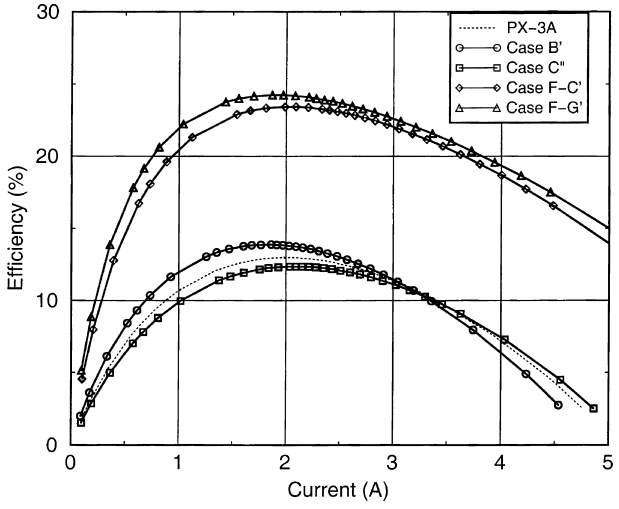

Fig. 9. The cell conversion efficiency ($T_{hot} = 1173$ K).

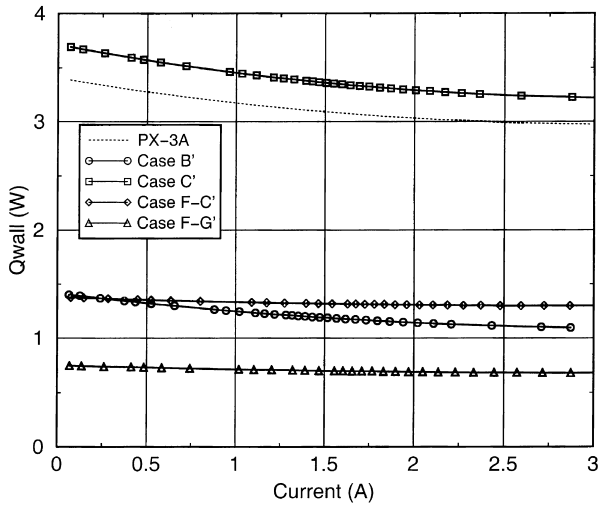

Fig. 12. Conducted heat to condenser through cell wall ($T_{hot} = 1023$ K).

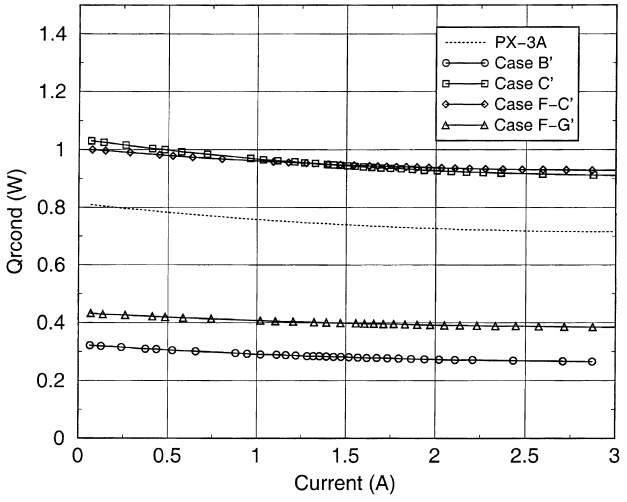

Fig. 13. Net heat radiation to condenser ($T_{hot} = 1023$ K).

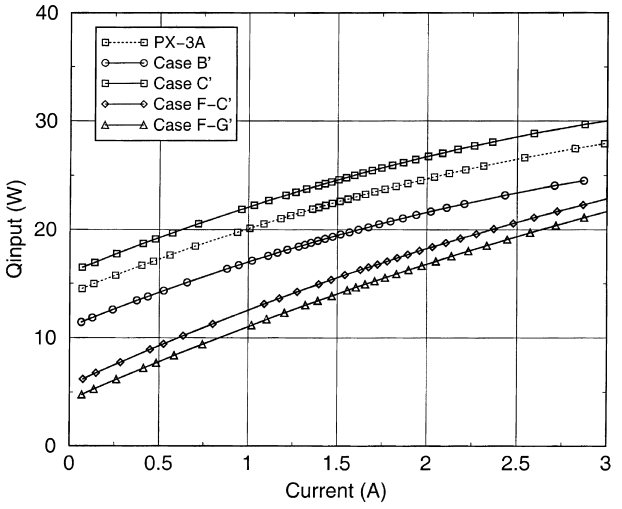

Fig. 14. The heat supplied to the AMTEC cell ($T_{hot} = 1023$ K).

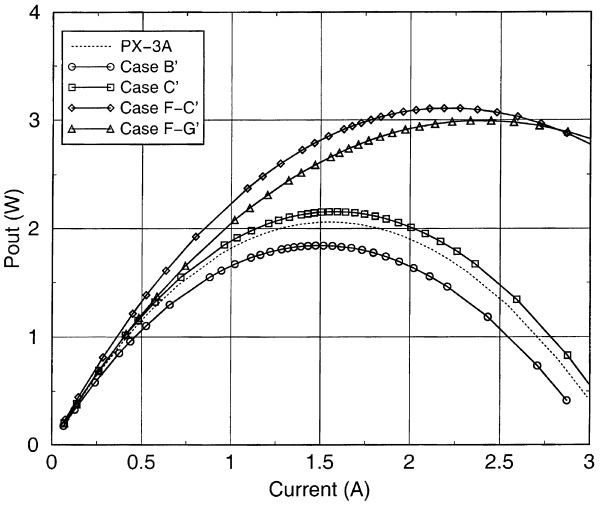

Fig. 15. The electrical power generated by the cell ($T_{hot} = 1023$ K).

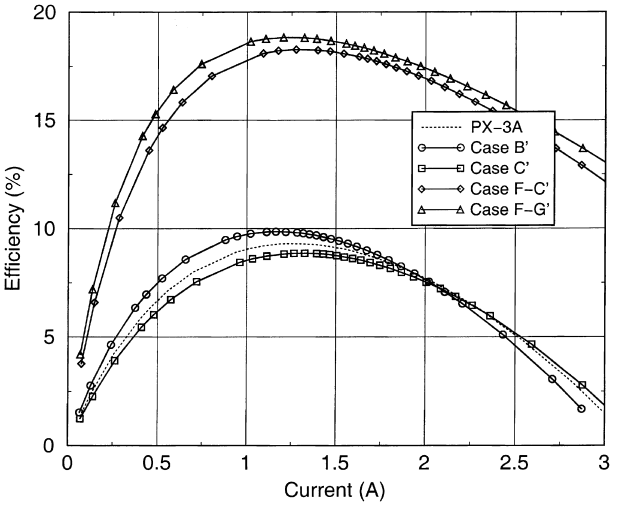

Fig. 16. The cell conversion efficiency ($T_{hot} = 1023$ K).

conversion efficiency reached to 13.76% . They increase by 46 and 48%, respectively, with the hot end temperature $T_{hot} = 1023$ K.

As mentioned before, experimental data for PX-3A cell, up to 18,000 h, show that the power generated by the cell decreases as the operating time increases. The power degradation occurs rapidly during the first 552 h, then slows down relatively. After 18,000 h of operating time PX-3A cell degrades by 48%, see Fig. 2 [29]. This power degradation results from various changes that occurred in the cell components during its operation. Studies show that the temperature independent exchange current and the BASE conductivity decrease with time [36–41]. Assuming first that the power degradation is directly related to, and is only due to the decrease in the temperature independent exchange current, the power output fitted to data for $R_{load} = 1\ \Omega$ is shown by long dashed curve in Fig. 2. The function used for the temperature independent exchange current is obtained by curve fitting technique with the experimental data and is given by

$$B = B_0 - 16\,t^{0.25}$$

where B_0 is initial the temperature independent exchange current (at $t = 0$) and t is the time. Using above function, the power degradation is found as 44.96% after 18,000 h. Next the degradation results with similar assumptions for BASE resistivity instead of the exchange current is shown by the dotted line in this figure. The function used for BASE resistivity as obtained by the curve fitting is given by

$$R_{base} = R_{base,o}(1 + 0.03\,t^{0.5})$$

The power drop is calculated as 31.20% by changing BASE resistivity. Using the same equations for the temperature independent exchange current and the BASE resistivity, the power degradations for case E–C′ for $R_{load} = 1\ \Omega$ are shown with dot-dashed and dashed lines respectively in Fig. 2. In

Table 6
Power degradation rate of AMTEC cell over 18,000 h

	Initial power output (W)	Final power output (W)	Degradation (%)
Observed	2.45	1.27	48.16
Curve fit (exchange current)	2.38	1.31	44.96
Curve fit (BASE resistivity)	2.34	1.61	31.20
Case E–C′ (exchange current)	3.35	1.82	45.67
Case E–C′ (BASE resisitivity)	3.29	2.18	33.74

these cases, the power degradations are found as 45.67 and 33.74%, respectively, see Table 6.

6. Conclusion

In this study, a number of changes for improving the AMTEC cell performance are introduced. The cell conversion efficiency can be increased with improved thermal isolation between the heat source (hot plate) and sink (condenser). Results show that the heat losses due to conduction can be reduced by using low thermally conducting material for cooler region components. The heat losses due radiation can be reduced by using relatively high reflective (small emissivity) surfaces. The heat losses in the axial direction along the cell wall and artery, and heat radiation to condenser have been shown to decrease by increasing cell height. Accordingly the electrical power output and the cell conversion efficiency are shown to increase. Also the electrical power output and the cell conversion efficiency have been demonstrated to increase by using highly thermally conducting material for hot region components of the cell and larger cross-section of the stud. The effect of the variation of cell diameter is formed to decrease cell conversion efficiency but to increase the electrical power output. However, both cell conversion efficiency and the electrical power output vary directly as the length of the electrode.

The higher electrical power output and cell conversion efficiency have been obtained by combining material and geometrical changes for the cell. The maximum electrical power output reached to 6.419 W for case E–C′, although it is 6.135 W for case E. The maximum cell conversion efficiency reached to 18.654% for case E–G′. It was 18.09% for case E. These results are obtained for $T_{hot} = 1173$ K. For $T_{hot} = 1023$ K, similar results are found. The maximum electrical power output and the maximum cell conversion efficiency reached to 3.007 W and 13.763%, respectively.

The cell generates higher electrical power output for case E–C′ all the way through 18,000 h of operating time than the observed value, see Fig. 2. The power degradation rate over this period improved for E–C′ cases compared with the observed value. The degradation rates are less than 46 and 34% for two approaches of case E–C′, whereas the observed data is 48%. It is therefore recommended to operate a prototype AMTEC cell with the parameters of the case E–C′ for improved efficiency, power output and degradation rate over the one in operating currently.

Acknowledgements

We are indebted to John Merrill for providing the latest AMTEC data before publication. This work is supported in parts by Center for Energy Research, Texas Technical University, Texas Advanced Technology Program under Grant Number 003644-091, and AFOSR Sub-contract 99-0832 CFDA #12.800.

References

[1] J.T. Kummer, N. Weber, U.S. Patent 3,458,356, assigned to Ford Motor Co (1968).
[2] N. Weber, Energy Conversion 14 (1974) 1.
[3] T.K. Hunt, N. Weber, T. Cole, in: Proceedings of the 10th Intersociety Energy Conversion Engineering Conference, Part 2, 1975, p. 231.
[4] T.K. Hunt, N. Weber, T. Cole, in: Proceedings of the 13th Intersociety Energy Conversion Engineering Conference, SAE, Warrandale, PA, 1978, p. 2001.
[5] A. Schock, in: Proceedings of the 15th Intersociety Energy Conversion Engineering Conference, SAE, Seattle, WA, 1980, p. 1032.
[6] T.K. Hunt, N. Weber, T. Cole, in: J.B. Bates, G.C. Ferrington (Eds.), Solid State Ionics, North Holland, Amsterdam, 1981, p. 263.
[7] G. Crosbie, G. Tennenhouse, J. Am. Ceram. Soc. 65 (1982) 187.
[8] T. Cole, Science 221 (1983) 915.
[9] C.P. Bankston, T. Cole, S.K. Khanna, A.P. Thakoor, in: M.S. El-Genk, M.D. Hoover (Eds.), Space Nuclear Power Systems 1984, Vol. II, Orbit Book Co., Malabar, FL, 1985, p. 393.
[10] R.M. Williams, S.K. Khanna, C.P. Bankston, A.P. Thakoor, T. Cole, J. Electrochem. Soc. 133 (1986) 1587.
[11] R.M. Williams, B.L. Wheeler, B. Jeffries-Nakamura, M.E. Loveland, C.P. Bankston, T. Cole, J. Electrochem. Soc. 135 (1988) 2736.
[12] R.K. Sievers, C.P. Bankston, in: Proceedings of the 23rd Intersociety Energy Conversion Conference, 3, 1988, p. 159.
[13] M.L. Underwood, D. O'Connor, R.M. Williams, B. Jeffries-Nakamura, C.P. Bankston, in: Proceedings of the 24th Intersociety Energy Conversion Engineering Conference, 6, Washington, DC, 1989, p. 2833.
[14] R.M. Williams, B. Jeffries-Nakamura, M.L. Underwood, B.L. Wheeler, M.E. Loveland, S.J. Kikkert, J.L. Lamb, J.T. Kummer, C.P. Bankstone, J. Electrochem. Soc. 136 (1989) 893.
[15] R.M. Williams, M.E. Loveland, B. Jeffries-Nakamura, M.L. Underwood, C.P. Bankston, H. Leduc, J.T. Kummer, J. Electrochem. Soc. 137 (1990) 1709.
[16] R.M. Williams, B. Jeffries-Nakamura, M.L. Underwood, C.P. Bankston, J.T. Kummer, J. Electrochem. Soc. 137 (1990) 1716.

[17] M.L. Underwood, D. O'Connor, R.M. Williams, B. Jeffries-Nakamura, M.A. Ryan, C.P. Bankston, J. Propulsion Power 8 (4) (1992) 878–882.
[18] T.K. Hunt, R.K. Sievers, J.F. Ivaneok, J.E. Pantolin, D.A. Butkiewicz, in: Proceedings of the 28th Intersociety Energy Conversion Conference, 1, 1993, p. 849.
[19] C.P. Bankston, A Critical Review of Space Nuclear Power and Propulsion 1984–1993, AIP Press, NY, 1994, pp. 443–457.
[20] J.F. Ivanenok III, R.K. Sievers, C.J. Crowley, AIChE Symp. Ser. 91 (1995) 356.
[21] M.J. Schuller, R.A. LeMire, K. Horner-Richardson, in: Proceedings of the 30th Intersociety Energy Conversion Conference, 3, 1995, p. 159.
[22] T.K. Hunt, R.K. Sievers, J.F. Ivanenok, in: Proceedings of the 30th Intersociety Energy Conversion Conference, 3, 1995, p. 145.
[23] M.A.K. Lodhi, Michael Schuller, Paul Housgen, in: M.S. El-Genk (Ed.), Proceedings of the Space Technology and Applications International Forum, AIP Press, NY, 1996, p. 1285.
[24] Q. Ni, J. Tong, Y. Kan, J. Wang, Y. Cui, in: Proceedings of the 32nd Intersociety Energy Conversion Conference, 97058, 2, 1997, p. 1180.
[25] A. Schock, H. Noravian, V. Kumar, C. Or, in: Proceedings of the 32nd Intersociety Energy Conversion Conference, 97529, 2, 1997, p. 1136.
[26] J.M. Merrill, M. Schuller, L. Huang, 15th STAIF, AIP Press, NY, 1998, p. 1613.
[27] J.M. Merrill, Clay Mayberry, 16th STAIF, AIP Press, NY, 1999, p. 1369.
[28] A. Schock, H. Noravian, C. Or, V. Kumar, AIP Conference Proceedings, No. 158, 1999, p. 1534.
[29] J.M. Merrill, private communication.
[30] T.J. Hendricks, C. Huang, in: Proceedings of the 33rd Intersociety Energy Conversion Conference, IECEC-98-407, Colorado Springs, CO, 1998.
[31] M.S. El-Genk, J.M. Tournier, R. James, C. Mayberry, 16th STAIF, AIP Press, NY, 1999, p. 1293.
[32] M.A.K. Lodhi, A. Daloglu, J. Power Sources 85 (2000) 203.
[33] M.A.K. Lodhi, A. Daloglu, J. Power Sources, in press.
[34] J.M. Tournier, M.S. El-Ghenk, M. Schuller, P. Hausgen, in: Proceedings of the 14th STAIF-97, 1997, p. 397.
[35] J.M. Tournier, M.S. El-Genk, L. Huang, M.J. Schuller, in: Proceedings of the 32nd Intersociety Energy Conversion Conference, 97378, 2, 1997, p. 1172.
[36] J.F. Ivanenok, R.K. Sievers, in: Proceedings of the 30th Intersociety Energy Conversion Conference, 1, 1997, p. 661.
[37] M.A. Ryan, R.M. Williams, M.L. Homer, W.M. Phillips, L. Lara, J. Miller, in: M.S. El-Genk (Ed.), Proceedings of the Space Technology and Applications International Forum, AIP Press, NY, 1995, p. 1607.
[38] M.A. Ryan, A. Kisor, R.M. Williams, in: Proceedings of the 29th Intersociety Energy Conversion Conference, 2, 1994, p. 877.
[39] R.M. Williams, A. Kisor, M.A. Ryan, J. Electrochem. Soc. 142 (1995) 4246.
[40] M.A. Ryan, R.M. Williams, M.L. Homer, V.B. Shields, S. Wright, L. Lara, J. Miller, in: M.S. El-Genk (Ed.), Proceedings of the Space Technology and Applications International Forum, AIP Press, NY, 1999, p. 1301.
[41] R.M. Williams, M.A. Ryan, M.L. Homer, L. Lara, K. Manatt, V. Shields, R.H. Cortez, J. Kulleck, in: M.S. El-Genk (Ed.), Proceedings of the Space Technology and Applications International Forum, AIP Press, NY, 1999, p. 1306.